

# Measurements of the hyperpolarizability tensor by means of hyper-Rayleigh scattering

V. Ostroverkhov, R.G. Petschek, and K.D. Singer  
*Dept. of Physics, Case Western Reserve University, Cleveland, OH 44106*

L. Sukhomlinova, R.J. Twieg S.-X. Wang and L.C. Chien  
*Liquid Crystal Institute and Dept. of Chemistry, Kent State University, Kent, Ohio 44242*

## Abstract

We describe improvements to our previously reported hyper-Rayleigh scattering technique to measure all rotational invariants of the first hyperpolarizability tensor. The full hyper-Rayleigh scattering tensor is expressed in terms of its rotationally invariant components leading to figures of merit corresponding to each of the rotationally invariant tensors. Using elliptically polarized incident light, the polarization state and intensity of the harmonic light is measured at a scattering angle of  $45^\circ$ . A new analytical fitting method is applied to the signal for two polarization measurements to determine the invariants. We have measured several chiral and non-chiral chromophores to determine the hyperpolarizability tensor to analyze the accuracy and to reveal structure property relationships related to the applicability of the chromophores as nonlinear optical materials. Results for a series of chiral chromophores and crystal violet are presented. *OCIS codes:* 160.4330 (Nonlinear optical materials), 190.0190 (Nonlinear optics), 190.4400 (Nonlinear optics, materials), 190.4710 (Optical nonlinearities in organic materials), 290.5840 (Scattering, molecules), 120.5820 (Scattering measurements).

## Introduction

Second-order nonlinear optics in organic materials has been the subject of considerable research with nearly all effort aimed at understanding and exploiting dipolar molecules containing delocalized electrons with electron withdrawing and/or donating substituents. [1] These compounds possess large molecular hyperpolarizabilities that have been utilized in polar macroscopic materials such as molecular crystals, poled polymers, and monomolecular films with polar noncentrosymmetric structures.[2] These compounds often exhibit a dominant one-dimensional character, and, as such, necessarily satisfy Kleinman (full-permutation) symmetry.[3] In this case, maximizing the nonlinear optical response often involves a large change in dipole moment between a dominant excited state and the ground state. The ground state dipole moment is usually also large and especially important in cases where electric field poling is required. The technique of electric field induced second harmonic generation (EFISH) is appropriate for determination of the molecular figure of merit for these materials. Molecular design of these materials is now a mature topic following decades of study.[4]

The molecular hyperpolarizability, however, has other components that are of equal interest. The hyperpolarizability,  $\beta_{ijk}$ , a third-rank tensor, describes the relevant nonlinear optical properties. According to group theory, this tensor can be described in part by rotationally invariant scalar figures of merit. A rank-one tensor, which transforms as a vector, describes the polar response described above, and its figure of merit is measured by EFISH. In the Kleinman symmetric regime, this vector and a third rank tensor, widely known as the octupolar component, fully describe the response. This octupolar component has been the subject of recent research, and molecular properties for efficient octupolar interactions have been elucidated.[5,6,7] In this case, however, EFISH is unable to measure the relevant figure of merit and hyper-Rayleigh scattering (HRS) is used instead.[5,8] The exploitation of the octupolar molecular response in macroscopic materials is not at all straightforward, but has been demonstrated using optical poling techniques.[6]

We have recently discussed an approach to fully characterize the molecular hyperpolarizability in the Kleinman-disallowed regime using HRS.[9] In the case of Kleinman symmetry breaking, seven tensors that transform like irreducible representations of the rotation group and the corresponding fifteen scalar figures of merit represent the parametric hyperpolarizability.[10,11] For second harmonic generation, four irreducible tensors contribute and there are 6 scalar figures of merit. As we describe elsewhere, this molecular response may be exploited in axially ordered materials such as liquid crystals and stretched polymers.[12] Kleinman-disallowed components necessarily involve multidimensional excitations, and thus open a new vista on the nonlinear optical response of organic molecules. Thus, the possibility of utilizing other components of the  $\beta$  tensor has motivated this work. In addition, full characterization of the hyperpolarizability along with quantum chemical calculations provides a method for studying the electronic structure of molecules.

In this paper, our aims are threefold. 1) We present improvements on our previously reported technique including a new analytical fitting method, and an experimental configuration capable of producing the maximum number of independent measured quantities, which we demonstrate to result in improved accuracy, 2) we build on previous work by extending HRS measurements of the scalar invariants to new chromophores that exhibit sizable Kleinman disallowed components, and 3) for the convenience of the reader, we also correct some errors in the theory that appeared in Eqs. 6, 12, 14, 18, 19, 20, 27, 28, 29 and 31 and Table 2 of our previous paper on this subject.[9] Results on new chromophores, both chiral and non-chiral are presented in order to help establish the accuracy of the technique and its application to the study of structure-property relationships in molecules possessing multidimensional charge transfer. The aspects and impact of chirality are discussed elsewhere.[12]

## **Theoretical approach**

Two optical fields  $E_1$  and  $E_2$  with frequencies  $\omega_1$  and  $\omega_2$  propagating in an isotropic solution of nonlinear optical molecules generate scattered light of frequency  $\omega_3 = \omega_1 + \omega_2$  with the intensity of the sum frequency defined by

$$I_{IL}^{w_3} = GNB_{IJKLMN}^2(\mathbf{w}_3; \mathbf{w}_1, \mathbf{w}_2) E_J^{w_1} E_K^{w_2} (E_M^{w_1})^* (E_N^{w_2})^* \quad (1)$$

where  $G$  includes the details of the experiment such as local field factors and geometry,  $N$  is the number density of the nonlinear molecules in the solution, and  $B^2$  is the square of the molecular hyperpolarizability averaged over all spatial orientations, which is the object of study in a parametric light scattering experiment.

The most efficient way of analyzing the  $B^2$  tensor utilizes the decomposition of the first order molecular hyperpolarizability tensor  $\beta$  into components irreducible under 3D rotation, as was mentioned above. This decomposition defines the maximum number of observable contributions to  $B^2$ . Thus, it becomes possible to write  $B^2$  as a sum of rotationally invariant tensors  $\Delta_{IJK,LMN}$  with scalar coefficients  $\beta^2$  that are the rotational invariants of the hyperpolarizability tensor  $\beta$ :

$$B_{IJK,LMN}^2 \equiv \langle \mathbf{b}_{IJK} \mathbf{b}_{LMN}^* \rangle = \sum_{\mathbf{L}} \Delta(\mathbf{L})_{IJK,LMN} \beta^2(\mathbf{L}) \quad (2)$$

The scalar coefficients represent figures of merit for each of the processes associated with the tensors,  $\Delta$ .

The invariant tensors  $\Delta_{IJK,LMN}$  can be constructed to correspond to the irreducible representations of the three-dimensional rotation group  $L=0, 1, 2, 3$ , contained in the  $\beta$  tensor. Thus, the index  $\mathbf{L}$  represents a set of indices including  $L$  – the weight (or rank) of the irreducible part, and  $\sigma$  and  $\sigma'$ , the type of index-permutation symmetry for the first and last three indices of  $\Delta_{IJK,LMN}$  (with values  $a$  for fully antisymmetric,  $s$  for fully symmetric, and  $m$  and  $m'$  for mixed representations that are symmetric and antisymmetric under exchange of last two indices respectively).

The construction of  $\Delta$  tensors can be greatly simplified by using the fact that the scattering medium is isotropic. In this case, the  $\Delta$  tensors (as well as any macroscopic characteristic of an isotropic system) have to be rotationally invariant. In the Cartesian representation, any rotationally invariant tensor can be composed of products of the elements of the symmetric unit tensor and totally antisymmetric tensor (the Kronecker  $\delta_{ij}$  and Levi-Civita  $\epsilon_{ijk}$  respectively), which are the only elementary invariant tensors. As a rank-6 tensor,  $B_{IJK,LMN}^2$  includes only 15 linearly independent products of three

Kronecker symbols (such as  $\mathbf{d}_{ij}\mathbf{d}_{kl}\mathbf{d}_{mn}$  and its permutations) one combination of which is conveniently written as the product of two Levi-Civita symbols. Use of the Levi-Civita symbols in some cases makes it easier to analyze the permutation symmetries of the tensors. The parts with particular permutation symmetries can be extracted by acting on the left and right indices of the tensor with appropriate projection operators constructed to satisfy certain permutation symmetries as follows:

$$\mathbf{P}_s = \frac{1}{6} \left[ 1 + (1 \leftrightarrow 2) + (1 \leftrightarrow 3) + (2 \leftrightarrow 3) + (1 \rightarrow 2 \rightarrow 3) + (1 \rightarrow 3 \rightarrow 2) \right]$$

$$\mathbf{P}_m = \frac{1}{6} \left[ 2 + 2(2 \leftrightarrow 3) - (1 \leftrightarrow 2) - (1 \leftrightarrow 3) - (1 \rightarrow 2 \rightarrow 3) - (1 \rightarrow 3 \rightarrow 2) \right]$$

$$\mathbf{P}_{m'} = \frac{1}{6} \left[ 2 - 2(2 \leftrightarrow 3) + (1 \leftrightarrow 2) + (1 \leftrightarrow 3) - (1 \rightarrow 2 \rightarrow 3) - (1 \rightarrow 3 \rightarrow 2) \right]$$

An antisymmetric operator is needed for parametric light scattering, but not for hyper-Rayleigh scattering. Two and three digit sequences are the cyclic notation denoting permutations of two and three indices. The operators are orthogonal to each other so that they extract projections of a tensor onto orthogonal subspaces of tensors with permutation symmetries  $s$ ,  $m$ , and  $m'$  standing for fully symmetric and two mixed representations defined above. The numerical constants assure the general property of orthogonal projection operators  $\mathbf{P}_i \mathbf{P}_j = \mathbf{P}_i \delta_{ij}$ .

Table 1 presents the 15 rotation invariant tensors with appropriate normalization coefficients calculated on the basis of the orthogonality condition:

$$\sum_{ijklmn=1}^3 \Delta(\mathbf{L})_{ijk,lmn} \Delta(\mathbf{L}')_{ijk,lmn} = \mathbf{d}_{\mathbf{L}\mathbf{L}'} \quad (3)$$

Using this normalization condition, one can define the rotation invariants  $\mathbf{b}^2(\mathbf{L})$  that are being determined in the experiment in terms of Cartesian components of the hyperpolarizability tensor (see Appendix A). The tensors are constructed according to the general decomposition of the tensor  $\beta$  (Eq.(2)).[12] By construction, all tensors obtained with the  $m'$  projection operator vanish in the case of undistinguishable incoming fields ( $\beta$  symmetric with respect to last two indices) so that only 6 invariant tensors contribute to hyper-Rayleigh scattering.

Since we are only considering hyper-Rayleigh scattering, we will confine our discussion to the case of identical input fields leaving out the rotationally invariant

tensors with  $a$  and  $m$  permutation symmetries. Combining the expressions for the scattered intensity  $I_L$  (Eq.(1)), the average square molecular polarizability  $B^2$  (Eq. (2)), and the definitions for invariant tensors  $\Delta$  (Table 1), one can write down the intensity of the scattered polarized light measured in HRS experiment solely as a function of the six scalar invariants of the hyperpolarizability tensor  $\mathbf{b}^2(\mathbf{L})$  (where  $\mathbf{L}=1ss, 1mm, 1sm+, 1sm-, 2mm, 3ss$ ) and the polarizations of incoming (fundamental) and outgoing (second harmonic) light:

$$I^{2w}(\hat{e}_i, \hat{e}_o) \propto (I^w)^2 \sum_{\mathbf{L}} \mathbf{b}^2(\mathbf{L}) \Delta(\mathbf{L})_{IJK,LMN} (\hat{e}_o^*)_I (\hat{e}_i)_J (\hat{e}_i)_K (\hat{e}_o)_L (\hat{e}_i^*)_M (\hat{e}_i^*)_N \quad (4)$$

$$I^w = |E^w|^2; \quad \mathbf{E}^w = \hat{e}_i E^w$$

An arbitrary elliptical polarization can be obtained by sending light through a linear polarizer and a  $1/4$ -wave plate with a particular orientation of their axes. In order to analyze the potential experiments, it is useful to calculate the contraction of  $\Delta(\mathbf{L})_{IJK,LMN}$  with the six polarization vectors. Eq. (4) then becomes a function of angles of the incoming and outgoing polarizers and  $1/4$ -wave plates  $\Delta_{\mathbf{L}}(\Omega_i, \Omega_o)$  and can be rewritten as

$$I^{2w}(\Omega_i, \Omega_o) = GN (I^w)^2 \sum_{\mathbf{L}} \mathbf{b}_{\mathbf{L}}^2 \Delta_{\mathbf{L}}(\Omega_i, \Omega_o) \quad (5)$$

where  $\Omega_i$  and  $\Omega_o$  denote sets of angles for incident and analyzed light. The angular functions  $\Delta_{\mathbf{L}}$ , which are the  $\Delta(\mathbf{L})_{ijk,lmn}$  contracted with the polarization vectors, are given by

$$\begin{aligned} \Delta_{1ss} &= c_{1ss} \frac{1}{9} \left[ AA^* + 4BB^* + 4\text{Re}(BA^*C) \right] \\ \Delta_{1mm} &= c_{1mm} \frac{4}{9} \left[ AA^* + BB^* - 2\text{Re}(BA^*C) \right] \\ \Delta_{1sm+} &= c_{1sm+} \frac{4}{9} \left[ AA^* - 2BB^* + \text{Re}(BA^*C) \right] \\ \Delta_{1sm-} &= c_{1sm-} \frac{-4i}{3} \left[ \text{Im}(BA^*C) \right] \\ \Delta_{2mm} &= c_{2mm} \frac{4}{9} \left[ AA^* + BB^* - 2\text{Re}(BA^*C) \right] + c'_{2mm} \frac{2}{3} \left[ 1 - CC^* \right] \\ \Delta_{3ss} &= c_{3ss} \frac{1}{3} \left[ 1 + 2CC^* \right] + c'_{3ss} \frac{1}{9} \left[ AA^* + 4BB^* + 4\text{Re}(BA^*C) \right] \end{aligned} \quad (6)$$

with  $A = \hat{e}_i \cdot \hat{e}_i$ ,  $B = \hat{e}_i \cdot \hat{e}_o^*$ ,  $C = \hat{e}_i \cdot \hat{e}_o$ , and the  $c$ 's are normalization constants.

Eqs. (5) and (6) describe how the intensity in the hyper-Rayleigh scattering experiment depends on molecular invariants and configuration of the experiment. Measurements for which the six trigonometric functions  $\Delta_{\mathbf{L}}$  are linearly independent make it possible to determine all six coefficients  $\mathbf{b}_{\mathbf{L}}^2$  e.g. by fitting the function (Eq. (5)) to the angular dependence of the intensity from the experiment. In the following section, we will discuss the definition for the input and output polarization vectors through the trigonometric functions of angles, the choice of the experimental configuration providing the most independent measurement of six invariants of  $\beta$ , and the procedure chosen for data analysis.

## Experiment configuration and data analysis

The hyper-Rayleigh scattering experiment configuration with arbitrary polarizations of the incident and scattered light, and scattering angle is shown in Figure 1. We need to create elliptical polarization states for the incoming and outgoing light by setting the polarizer and analyzer angles in this figure. The unit vectors of the incident and outgoing polarizations are then given by

$$\begin{aligned}\hat{e}_i &= \cos(\mathbf{g} - \mathbf{a}_i)(\hat{x} \sin \mathbf{g} + \hat{y} \cos \mathbf{g}) + i \sin(\mathbf{g} - \mathbf{a}_i)(\hat{y} \sin \mathbf{g} - \hat{x} \cos \mathbf{g}) \\ \hat{e}_o &= \cos(\mathbf{g} - \mathbf{a}_o)[(\hat{x} \cos \mathbf{q} + \hat{z} \sin \mathbf{q}) \sin \mathbf{g} + \hat{y} \cos \mathbf{g}] + \\ &\quad + i \sin(\mathbf{g} - \mathbf{a}_o)[\hat{y} \sin \mathbf{g} - (\hat{x} \cos \mathbf{q} + \hat{z} \sin \mathbf{q}) \cos \mathbf{g}]\end{aligned}\quad (7)$$

Here,  $\alpha_i$  and  $\alpha_o$  are the angles of the input and output polarizers' axes and  $\gamma_i$  and  $\gamma_o$  are the angular positions of the respective quarter-wave plates relative to the  $\hat{x}$ ,  $\hat{y}$ , and  $\hat{z}$  directions, and  $\theta$  is the scattering angle. The angles  $\alpha$  and  $\gamma$  are measured from  $\hat{y}$ -axis counterclockwise looking in the direction of the propagation of the beam.

Analyzing Eqs. (7) together with Eqs. (6), one can define configurations of the experiment that are most appropriate for distinguishing the contributions of the six rotation invariants, leaving out the cases where the functions are dependent. For example, an experiment measuring linearly polarized outgoing light is clearly not suitable for the measurements of the six invariants: the condition  $\mathbf{a}_o = \mathbf{g}$  makes the output polarization

vector real, and leads to  $B=C$  in Eq. (6) so that the angular functions  $\Delta_L$  can be expressed in terms of only 5 independent functions ( $1, AA^*, BB^*=CC^*, BA^*C$  and  $B^*AC^*$ ), which also makes them linearly dependent. The same problem occurs for linearly polarized incident light. The condition  $\hat{e}_i = \hat{e}_i^*$  implies  $A = \hat{e}_i \cdot \hat{e}_i = 1$ , which again reduces the number of independent functions involved. Also  $AA^*$  must be linearly independent from unity, which implies that at least two input polarizations with *different* ellipticities must be used.

It is also straightforward to see that  $90^\circ$ -scattering is not appropriate for this experiment. The case of  $90^\circ$ -scattering has been widely used in HRS experiments for systems presumed to have Kleinman symmetry. For  $\mathbf{q} = 90^\circ$ , the  $\hat{x}$ -component of outgoing polarization vanishes (Eq. (7)). Since  $\hat{e}_i$  does not have a  $\hat{z}$ -component, only the  $\hat{y}$ -components of both vectors contribute to their dot products  $B$  and  $C$ . The polarization vectors are only defined up to an arbitrary phase factor. We can chose this phase factor such that the  $\hat{y}$ -components of  $\hat{e}_i$  and  $\hat{e}_o$  are real, which makes  $B$  and  $C$  real and equal, which consequently leaves only four independent functions ( $1, BB^*=B^2=CC^*=C^2, BA^*C$  and  $B^*AC^*$  while  $AA^*=(BA^*C)(B^*AC^*)/B^2C^2$ ). Finally, the  $90^\circ$ -scattering experiment combined with linearly polarized fundamental and harmonic light retains only two observables ( $1=AA^*$  and  $BB^*=CC^*=BA^*C=B^*AC^*$ ). This result agrees with previous work where the depolarization ratio is measured assuming Kleinman symmetry(e.g. [6]). In this previous work, it has been pointed out that the depolarization ratio measurement is suitable for determining the two possible rotation invariants for the fully symmetric  $\beta$  tensor (Kleinman allowed vector and octupole). However, if there is a significant contribution from Kleinman-disallowed components, a more general configuration is necessary, and the depolarization ratio serves as a source of complimentary information (see Appendix B).

We used an analysis similar to, but more involved than the one we have discussed above to choose the most appropriate configuration for our measurements. The scattering angle has been chosen to be  $45^\circ$ . Any scattering angle other than  $90^\circ$  has, in principle, a sufficient number of observables, but  $45^\circ$  was convenient from technical point of view. Angles close to forward and backward scattering are *theoretically* superior, provided that

the experimental difficulties associated with low angle scattering can be obviated. The incident polarization was taken to be  $90^\circ$  (lying in the scattering plane). Varying this polarization is technically difficult. The other three angles  $\gamma_i$ ,  $\alpha_o$ , and  $\gamma_o$  are left free to vary in the experiment. Fourier analysis of the expression  $AA^*$ ,  $BB^*$ ,  $CC^*$  shows that there are in general seven Fourier components that comprise these functions when the outgoing polarization is fixed and the incoming polarization is varied from linear through elliptical to circular by rotating the incoming  $1/4$ -wave plate (constant,  $\sin/\cos(2\gamma_i)$ ,  $\sin/\cos(4\gamma_i)$ , and  $\sin/\cos(6\gamma_i)$ ). The other option of fixed incoming polarization and varying the polarization of the analyzed second harmonic light returns fewer Fourier components. So, the angle  $\gamma_i$  was chosen as the experimentally independent variable. In addition, as a complete determination of all the scalar invariants requires the determination of six different constants, this implies that this rotation is the only possible way to determine all these invariants in a single experiment. As we see below, two experiments are needed even if  $\gamma_i$  is the independent variable.

Even though Eq. (7) defines the polarizations through parameters used in the experiment, it is more convenient for the purposes of this analysis to rewrite them in the following form:

$$\hat{e}_i = \frac{\exp(i\mathbf{y})}{\sqrt{2}} \left[ \hat{x}(i - \cos 2\mathbf{g}) + \hat{y} \sin 2\mathbf{g} \right] \quad (8)$$

$$\hat{e}_o = a\hat{z} + b \left[ \cos \mathbf{k}(\hat{x} \cos \mathbf{f} + \hat{y} \sin \mathbf{f}) + i \sin \mathbf{k}(-\hat{x} \sin \mathbf{f} + \hat{y} \cos \mathbf{f}) \right]$$

In the first expression of Eq. (8), the polarization of the incident laser light is horizontal ( $\alpha_i=90^\circ$ ,  $\mathbf{g} \equiv \mathbf{g}$ ). In the second expression, the  $xy$ -plane component of  $\hat{e}_o$  is separated from the  $z$ -component since the latter contributes quite differently to the scattered intensity. The  $xy$  part is represented as a generalized complex unit vector multiplied by a (complex) magnitude  $b$ . The angles  $\kappa$  and  $\phi$  give the ellipticity and orientation of the outgoing polarization in the  $xy$  plane. The angles can be always related to  $\alpha_o$  and  $\gamma_o$  by trigonometric equalities that can be resolved for one pair of angles when the other is given. Finally,  $\psi$  is a phase that can be factored out and does not contribute to the final Eq. (6) as all the terms contain as many  $\hat{e}_i$  as  $\hat{e}_i^*$  so that the phase multipliers

cancel out. Now, the auxiliary functions that constitute the angular functions (Eq. (6)) can be written in terms of new variables:

$$\begin{aligned}
AA^* &= \frac{1}{2}(1 + \cos 4\mathbf{g}) \tag{9} \\
BB^* &= \frac{b^2}{4}(2 + \cos 2\mathbf{k}\cos 2\mathbf{f} + \cos 4\mathbf{g}\cos 2\mathbf{k}\cos 2\mathbf{f} - \sin 4\mathbf{g}\cos 2\mathbf{k}\sin 2\mathbf{f} - 2\sin 2\mathbf{g}\sin 2\mathbf{k}) \\
CC^* &= \frac{b^2}{4}(2 + \cos 2\mathbf{k}\cos 2\mathbf{f} + \cos 4\mathbf{g}\cos 2\mathbf{k}\cos 2\mathbf{f} - \sin 4\mathbf{g}\cos 2\mathbf{k}\sin 2\mathbf{f} + 2\sin 2\mathbf{g}\sin 2\mathbf{k}) \\
BA^*C &= \frac{b^2}{4}\{1 + \cos 2\mathbf{k}\cos 2\mathbf{f} + \cos 4\mathbf{g}(1 + \cos 2\mathbf{k}\cos 2\mathbf{f}) - \sin 4\mathbf{g}\cos 2\mathbf{k}\sin 2\mathbf{f} - \\
&\quad - \frac{i}{2}[(\cos 2\mathbf{g} - \cos 6\mathbf{g})\cos 2\mathbf{k}\cos 2\mathbf{f} + (\sin 2\mathbf{g} + \sin 6\mathbf{g})\cos 2\mathbf{k}\sin 2\mathbf{f}]\}
\end{aligned}$$

Substituting Eq. (9) into Eqs. (6) and (5) gives an expression for the total scattered intensity as a trigonometric function of variable  $\gamma$  and parameters  $\kappa$  and  $\phi$ :

$$I^{2w}(\mathbf{g}, \mathbf{b}, \mathbf{k}, \mathbf{f}) = GN(I^w)^2 \sum_{n=0,2,4,6} \left[ a_n(\mathbf{b}^2, \mathbf{k}, \mathbf{f}) \cos n\mathbf{g} + b_n(\mathbf{b}^2, \mathbf{k}, \mathbf{f}) \sin n\mathbf{g} \right] \tag{10}$$

The trigonometric series form of Eqs. (10) suggests a way of analyzing the data through the Fourier transform. Fourier components composing the scattering intensity signal  $a_n$  and  $b_n$  are (linear) functions of invariants  $\mathbf{b}_L^2$

$$\{a, b\}_n(\mathbf{b}_L^2) = \sum_L \mathbf{A}(\mathbf{k}, \mathbf{f})_{n,L} \mathbf{b}_L^2; \quad n = 1 \mathbf{K} 7$$

and can be fitted simultaneously to Fourier components  $q_n$  extracted from the experimental signal. The  $\mathbf{c}^2$  is a simple quadratic form of the parameters of the fit that are being sought  $\mathbf{b}_L^2$ :

$$\mathbf{c}^2 = \sum_n (q_n - \mathbf{A}_{n,L} \mathbf{b}_L^2)^2$$

It can be readily expanded into form:

$$\mathbf{c}^2 = \mathbf{M}_{L,L'} \mathbf{b}_L^2 \mathbf{b}_{L'}^2 - 2\mathbf{U}_L \mathbf{b}_L^2 + const; \quad \mathbf{M}_{L,L'} = \mathbf{A}_{n,L} \mathbf{A}_{n,L'}; \quad \mathbf{U}_L = q_n \mathbf{A}_{n,L}.$$

Then, to minimize  $\mathbf{c}^2$  one has to solve a linear equation by inverting the (6×6) matrix

$\mathbf{M}_{L,L'}$ :

$$\frac{\partial}{\partial (\mathbf{b}_L^2)} \mathbf{c}^2 = 2\mathbf{M}_{L,L'} \mathbf{b}_{L'}^2 - 2\mathbf{U}_L = 0 \Rightarrow \mathbf{b}_L^2 = (\mathbf{M}^{-1})_{L,L'} \mathbf{U}_{L'}$$

The invariants can be determined only if the matrix  $\mathbf{M}_{L,L'}$  is not singular.

Eq. (10) also supplies a useful method to check for systematic errors and to check and analyze for the statistical errors. Specifically Fourier components of the data other than those included in Eq. (10) should consist only of noise. Thus looking to see if they are approximately constant assures that there are no systematic errors of certain types. They also give a scale for the statistical error. Such comparisons have been made for all the data presented below.

Despite the seven Fourier components,  $\mathbf{M}_{LL}$  is singular for any single experiment, because not all of the seven functions  $a_n$  and  $b_n$  are independent. In particular, three of them ( $a_2$ ,  $a_6$  and  $b_6$ ) are proportional to each other so that there are only five components that carry independent information. As a consequence, any single experiment is not sufficient and at least two experimental runs with different polarizations of outgoing light have to be analyzed together to find all six of the invariants. The least-square analysis is identical to one described above with  $\mathbf{c}^2$  taken to be a sum for two experiments  $\mathbf{c}_{ex1}^2 + \mathbf{c}_{ex2}^2$  that provides *simultaneous* fit of twice as many experimental points. The matrix  $\mathbf{M}_{LL}$  is not generally singular for two experimental runs with different output polarizations ( $\mathbf{k}_1, \mathbf{f}_1$  and  $\mathbf{k}_2, \mathbf{f}_2$ ), although some particular configurations (.e.g. linear output polarization) are singular even in this case.

When the output optics is rotated between the runs, the total intensity may change, thus distorting the fit. In order to avoid additional errors that may occur as a result of using the data from two independent measurements in the same fit, we introduced another variable, the ratio of the total intensities in the two experiments, in addition to the six rotation invariants as variables of fit. Ten independent Fourier components from two runs of the experiment allow determination of all the invariant scalars as well as this additional parameter. Analysis of many experiments showed that the ratio is close to unity (equal to unity within statistical error) so that, in practice, the additional parameter has little impact.

This approach to data analysis allows analysis of choices of the two experiments that will ensure the minimal errors in fitting parameters. The errors due to statistical fluctuations of experimental data are defined by covariance matrix:

$$\langle \mathbf{b}_i^2 \mathbf{b}_j^2 \rangle_c = \langle \mathbf{M}_{i,m}^{-1} \mathbf{U}_m \mathbf{M}_{j,l}^{-1} \mathbf{U}_l \rangle_c = \langle q_k q_{k'} \rangle_c \mathbf{M}_{i,m}^{-1} \mathbf{A}_{k,m} \mathbf{M}_{j,l}^{-1} \mathbf{A}_{k',l}$$

Assuming that there is no correlation in the statistical error of different data points, the covariance matrix is given by:

$$\langle q_k q_{k'} \rangle_c = \Delta q^2 \mathbf{d}_{kk'} \quad \Rightarrow \quad \langle \mathbf{b}_i^2 \mathbf{b}_j^2 \rangle_c = \mathbf{M}_{i,m}^{-1} \mathbf{M}_{m,l} \mathbf{M}_{j,l}^{-1}.$$

The size and orientation of the standard deviation volume is defined by eigenvalues and eigenvectors of the covariance matrix. Varying the parameters  $\mathbf{k}_1, \mathbf{f}_1$  and  $\mathbf{k}_2, \mathbf{f}_2$  and comparing the largest eigenvalues of  $\langle \mathbf{b}_i^2 \mathbf{b}_j^2 \rangle_c$ , we have found the several highly reliable configurations for the two experiments for which the largest eigenvalue is relatively small. The set of experiments with  $\mathbf{k}_1 = \frac{\mathbf{P}}{8}$ ,  $\mathbf{f}_1 = \frac{\mathbf{P}}{8}$  and  $\mathbf{k}_2 = \frac{\mathbf{P}}{2}$ ,  $\mathbf{f}_2 = \frac{\mathbf{P}}{8}$  appears to be a good choice, with the largest eigenvalue close to its minimum value. These angles correspond to  $(\mathbf{a}_o)_1 = 57.8^\circ$ ;  $(\mathbf{g})_1 = 75.25^\circ$  and  $(\mathbf{a}_o)_2 = (\mathbf{g})_2 = -30.4^\circ$ . There is a reasonably large region around these parameters in which the largest eigenvalue is close to that achieved for these values.

Our new improved data analysis method let us perform an analytical search for the optimal experiment configuration and proved to be a reliable way to find the rotational invariants  $\mathbf{b}_L^2$ . The algorithm was tested with simulated data obtained using a Monte-Carlo calculation. Both the invariants and the error bars were consistent with the original values used in the simulation. The method certainly does not have the convergence problems that are often associated with a multi-parameter search fit, as  $\chi^2$  is bilinear in all but one variable (the intensity ratio of the two experiments). As this single variable in which the fit is not bilinear is essentially known *a priori* the  $\chi^2$  surface usually (always in our experience) has a single minimum. The fitting program is also much faster than a generalized gradient search non-linear curve fit.

## Measurements and results

The experimental setup is shown on Figure 2. An optical parametric oscillator pumped by Nd:YAG Q-switched laser serves as a source of 3.5ns pulses tunable through

the near infrared with energy  $\sim 1.5\text{-}2$  mJ/pulse. Spatial filtering of the OPO output beam was required to carry out these measurements. The light passes through a polarizer and Berek compensator set to  $\lambda/4$  retardation for the current wavelength. An ordinary permanent  $1/4$ -wave retarder may be also used, although using a compensator makes switching from one wavelength to another much easier. The compensator is mounted on a rotation stage controlled by the data acquisition computer. Then, the fundamental light is focused (focal length 5cm) into a right-angle triangular cell that contains the filtered sample solution. Scattered second harmonic light is collected with a large-aperture aspherical lens (focal length 2.5cm). The collimated beam passes through a quarter-wave plate for frequency-doubled light, analyzer, and is finally collected on the photomultiplier tube of the “signal” channel with fundamental frequency being blocked with appropriate filters. A fraction of the laser light reflected from a beamsplitter is focused on a quartz crystal, which generates the second harmonic light which is used as a reference to eliminate shot-to-shot power variations (“reference” channel).

It has been pointed out that the presence of multiphoton fluorescence may become a considerable source of errors in HRS experiments [13, 14, 15]. This may lead to gross overestimates of the absolute values of hyperpolarizability as well as distort the information about the symmetry of the molecules when the polarization measurements are performed as the polarization content of fluorescence may differ from that for the second harmonic. In our study, we measured the spectral content of the light scattered from each substance to assure the dominance of the second harmonic light over the fluorescent background. UV-VIS absorption spectra of the solutions were also measured in order to take into account linear absorption losses at the wavelength of the harmonic light. Figure 3 depicts a typical spectrum of scattered light. For the solutions with significant optical density at  $\lambda_{\text{SH}}$ , the concentration of the chromophore was chosen such that the output signal is maximum for a given geometry of the setup (the tradeoff is achieved with the concentration that gives extinction of  $\sim \exp(-1)$  on the average length of light propagation).

We have performed the polarization HRS measurements described above for a series of organic molecules (Figure 4). The invariants determined from the experiment of HRS are shown in Table 2. The polar plots of typical data points from the two experimental runs

together with fitted curve for pNA, Q-BNH, and crystal violet are shown in Figure 5. Table 3 presents the figures of merit of the four irreducible parts of  $\beta$  in absolute units which make comparison more straightforward. The magnitude is referenced to EFISH measurements which yield the  $1s$  component directly:

$\mathbf{m}\mathbf{b}_{EFISH} = \frac{1}{3}(\mathbf{b}_{ijj} + \mathbf{b}_{jjj} + \mathbf{b}_{jji})\mathbf{m} \equiv \mathbf{b}^{1s} \cdot \mathbf{R}$ . In a molecule like pNA, the angle between permanent dipole moment  $\mathbf{m}$  and  $\mathbf{b}^{1s}$  has to be zero so that the value of  $\beta$  from EFISH may be used for scaling all the other components. We used the value

$\mathbf{b}_{pNA-EFISH} = 12 \cdot 10^{-30} esu$  at 1580nm from Ref. 114 of reference [4] scaled appropriately to our working wavelengths. The figure of merit in the Table 3 is defined by

$$\|\mathbf{b}_{1ss}\| \equiv \sqrt{\mathbf{b}_{1ss}^2} = \sqrt{c_{1ss} \mathbf{b}^{1s} \cdot \mathbf{b}^{1s}} = \sqrt{\frac{\sqrt{3}}{5}} |\mathbf{b}_{EFISH}| .$$

The absolute values of hyperpolarizability for different compounds were extracted from concentration measurements using the external reference scheme.[9]

## Results and discussion

The well-known molecule *p*-nitroaniline (pNA, 1) was measured as a reference and to help check the accuracy of our technique. It is generally considered to be nearly a "one dimensional" molecule, but quantum chemical calculations by Lalama and Garito do indicate small off-diagonal components.[16] Indeed, Tables 2 and 3 indicate that the contribution from Kleinman disallowed parts ( $1sm^+$ ,  $1sm^-$ , and  $2mm$ ) are relatively small. In Appendix A, we express the measured invariants in terms of Cartesian components, including special symmetry cases. In the case of pNA, we have a two-dimensional system having  $C_{2v}$  symmetry, so that the only nonzero components are  $\mathbf{b}_{zzz}$ ,  $\mathbf{b}_{zxx}$ , and  $\mathbf{b}_{xxz}$ . In this case, the Kleinman disallowed components become proportional to one another with the ratio  $\mathbf{b}_{1mm}^2 / \mathbf{b}_{2mm}^2 = \sqrt{\frac{5}{3}} \approx 1.3$ . (Note that our normalization in this paper is different than that of the literature.[5]) We do not find this in our results, with the  $1mm$  component being a bit larger than expected. However, our error bars indicate that these components are at the lower level of measurability, so a small systematic error may be contributing. Further experiments and quantum chemical calculations can help establish the accuracy here more firmly.

In Appendix B, we have calculated how the 90° scattering depolarization ratio can be calculated from our data. Depolarization ratios for pNA have been reported in the literature, and here we have determined a value of  $3.4 \pm 0.8$ , which is in reasonable agreement with the rather uncertain values in the literature ( $4.3 \pm 0.3$ ,  $4.9 \pm 0.2$ ). [14,17] Our unexpectedly large value for the *Imm* component here tends to lower the ratio as calculated from our results.

We can make more definite conclusions regarding the accuracy of the Kleinman allowed components. In the limit of purely a linear molecule (only  $\mathbf{b}_{zzz} \neq 0$ ), the Kleinman disallowed components vanish, and the nonzero rotation invariants with our normalization are

$$\mathbf{b}_{1ss}^2(1D) = \frac{\sqrt{3}}{5} \mathbf{b}_{zzz}^2; \quad \mathbf{b}_{3ss}^2(1D) = \frac{2}{5\sqrt{7}} \mathbf{b}_{zzz}^2.$$

This makes the ratio of octupolar to dipolar part given by,

$$\frac{\mathbf{b}_{3ss}^2}{\mathbf{b}_{1ss}^2} = \frac{2}{\sqrt{21}} \approx 0.436$$

Previous quantum chemical calculations have indicated that pNA is not strictly one-dimensional. Our measurements for pNA using the Kleinman allowed terms yields the ratio  $\approx 0.54$  that corresponds to  $\mathbf{b}_{zxx}/\mathbf{b}_{zzz} \approx -0.04$ , which is reasonable in light of the calculations of Lalama and Garito.[16]

Compounds **2-6** are camphorquinone derivatives. Camphorquinone was chosen as a basic chiral structure in our development of chiral nonlinear optical materials because its derivatives were known to have large optical rotatory power.[9] In this previous work, we have experimentally verified the large specific rotation. Quantum chemical calculations were also presented indicating that the chirality allows for multidimensional charge transfer around the camphor moiety to the acceptor, which was thought plausibly to increase the Kleinman disallowed components of the hyperpolarizability tensor. However, such *three* dimensional delocalization did not appear in light of [9] or of this work to be essential to the Kleinman disallowed components. Compound **2** is the basic structure, while the compounds **3** and **4** were synthesized to investigate the role of the acceptor strength on the various components. The compounds with dicyanovinyl acceptors have their linear absorption wavelength

shifted towards red and the  $I_{ss}$  (Kleinman allowed vector part) hyperpolarizability is considerably larger than that for compound **2**. The nature of the in-plane and out of plane electron transfer in compounds **2** and **3** is expected to be similar while that of compound **4** is expected to be different. This is because the location of the donor and the acceptor have been exchanged so that the two conformations **3** and **4** have different out-of-plane geometry. [18] However, in these cases at least, it is apparent that the stronger acceptor does not significantly enhance the Kleinman disallowed components.

Compound **5** was made to have longer  $\pi$ -conjugation. The effect of this modification is a substantial enhancement of the Kleinman allowed components, but the Kleinman disallowed components are not greatly affected. Thus, it appears that the substitution on the portion of the molecule (acceptor end) distant from the multidimensional moiety (donor end) does not greatly affect the Kleinman disallowed components. This supports the close connection between multidimensional charge transfer and the Kleinman disallowed components.

Compound **6**, Q-BNH, is a dimer counterpart of the basic chiral material **2**. This chromophore contains both a chiral center and the so-called  $\Lambda$ -structure (acceptor-donor-acceptor or donor-acceptor-donor). Others have reported Kleinman symmetry breaking in other  $\Lambda$ -shaped molecules.[14] We found that the  $2mm$  component, for example, in Q-BNH has a figure of merit about 50% higher than that of compound **2**. Note that  $\|\mathbf{b}_{2mm}\|$  is about two times as large as the vector part of pNA. Such molecules are also expected to have a large ( $90^\circ$ ) angle between the transition moment,  $\mu$  and the difference in the dipoles of the ground and first excited states,  $\Delta\mu$ . This is because either the highest occupied or lowest unoccupied molecular orbital is expected to be odd under reflection of the  $\Lambda$ , e.g. to have a node at the apex of the  $\Lambda$  while the other is expected to be even e.g. to have an antinode. Hence, the transition matrix element should be horizontal (in the usual orientation of a  $\Lambda$ ). However, this change is also expected to result in vertical motion of partial charge from the donor(s) to the acceptor(s). It is plausible that a large angle (in this case  $90^\circ$ ) between two vectors, which characterize different aspects of the first excited state, should be a reasonable measure of the multidimensional delocalization of electrons required for large Kleinman disallowed components. Clearly this is not the

only measure of multidimensional delocalization. Other measures are needed in chromophores like crystal violet (compound 8) with degenerate or nearly degenerate excited states. However, we show elsewhere that this condition is a good and simple measure of multidimensionality when the Kleinman disallowed components are not too small relative to the Kleinman allowed terms, and the first excited state dominates the Kleinman allowed nonlinear optical properties.[12] Compound 7 has a more rigid steroidal structure with multiple chiral centers. This molecule also exhibits Kleinman disallowed components.

Most interesting, however, are measurements of crystal violet (CV – 8). Here we distinctly see large Kleinman disallowed components. Previous measurements have all assumed Kleinman symmetry.[5, 8,14,15,19,20] However, one study indicated some peculiar results which would be, at least, partly explained by our measurements which do not assume Kleinman symmetry, and indeed show strong Kleinman symmetry breaking.[19] Octupolar (3ss) and Kleinman disallowed 2mm terms are allowed by the (naively expected)  $D_3$  (32) symmetry of this molecule. As we discuss in Appendix A, the  $I_{ss}$  or vector part is not allowed within this naively expected symmetry, but is observed.

These results support recent measurements and calculations suggesting symmetry breaking of the ground state of CV molecules [21,22] at least in certain solvents. It has been pointed out that the symmetry of the molecules can be lowered from  $D_3$  to  $C_3$ ,  $C_2$ , or  $C_1$  or changed to  $C_{2v}$ . These are all plausible symmetries for CV other than  $D_3$  and all allow for the existence of the vector components of  $\beta$  which would be in agreement with our results. As shown in Table 4, we observed a clear solvent dependence of the ratios of the rotational invariants confirming the role of the solvent in symmetry altering interactions.

We are also able to further establish the accuracy of our results by considering the depolarization ratio (as one would measure at  $90^\circ$  scattering) which we have calculated in Appendix B. We find that the derived depolarization ratio for CV of  $D = I_p/I_\perp \approx 1.5 \pm 0.3$  is in excellent agreement with that reported by others. [6,13,14].

Finally, the figures of merit for the  $\beta$  for CV are more than an order of magnitude larger than those of pNA. Such a huge contribution from the  $2mm$  part, for example, makes it reasonable to expect that CV or related chiral compounds could be effectively

used in systems with the macroscopic nonlinearity activated by means of an axial chiral system.[12] Of course, in addition to multi-dimensional electron delocalization it is a requirement for Kleinman disallowed components of  $\beta$  is that the system should not be well approximated by a static system in which e.g. all frequencies are small in comparison to that of the light absorbed in the transition from the ground to the first excited state. In the case of CV we are in the anomalous dispersion region e.g. the frequency of the fundamental is below and that of the second harmonic is above the first absorption band. It is again intuitive and is discussed in more detail elsewhere that this region should have relatively large Kleinman disallowed terms in  $\beta$ .

## Conclusions

We have described an improved experimental technique to determine the full hyperpolarizability tensor in the Kleinman symmetry breaking regime including a new analytic least square fitting technique. A polarization dependent hyper-Rayleigh scattering experiment with a scattering angle of  $45^\circ$  allows measurement the figures of merit corresponding to the four irreducible parts of  $\beta$  in case of second harmonic generation. At least a two-dimensional structure is necessary for Kleinman disallowed contributions to be observed. However, three-dimensional delocalization of electrons, which is required for optical rotatory power is not required. Specifically, camphorquinone derivatives – which have large optical rotatory powers – do not have large Kleinman disallowed terms. However two dimensional delocalization and specifically  $\Lambda$ -shaped molecules with two acceptors and a donor (or vice versa) have been seen to have substantial Kleinman disallowed parts of  $\beta$ . Crystal violet, which has a rather different structure and is measured in the anomalous dispersion region, also exhibits very strong Kleinman symmetry breaking. We also confirm distortion of crystal violet from the expected  $D_3$  shape but have no evidence whether or not this distortion (which makes the propeller more like a  $\Lambda$ ) is required for a large Kleinman disallowed hyperpolarizability. Our hyper-Rayleigh scattering results show that some molecules have appreciable Kleinman disallowed hyperpolarizabilities. Such multidimensional molecules may find application in forming nonpolar macroscopic materials with large second-order nonlinear optical responses.

## Acknowledgements

The authors wish to thank Dr. Paul Cahill of Exciton, Inc. (formerly of Sandia National Laboratories) for the Q-BNH material. This work was supported by the National Science Foundation through the ALCOM (Advanced Liquid Crystalline Optical Materials) Science and Technology Center (grant #DMR89-20147).

## Appendix A

The orthonormality of the invariant tensors  $\Delta(\mathbf{L})_{IJK,LMN}$  that are defined by equation (3) can be used to specify the meaning of the rotation invariants  $\mathbf{b}^2(\mathbf{L})$  in equation (2). Multiplying both sides of the equation by  $\Delta(\mathbf{L}')_{IJK,LMN}$  and summing over repeating indices we get for the right-hand side:

$$\sum_{\mathbf{L}} \sum_{\substack{IJK \\ LMN}} \Delta(\mathbf{L}')_{IJK,LMN} \Delta(\mathbf{L})_{IJK,LMN} \mathbf{b}^2(\mathbf{L}) = \sum_{\mathbf{L}} \mathbf{d}_{\mathbf{L}} \cdot \mathbf{b}^2(\mathbf{L}) = \mathbf{b}^2(\mathbf{L}') \quad (11)$$

while the left-hand side is

$$\Delta(\mathbf{L}')_{IJK,LMN} \langle \mathbf{b}_{IJK} \mathbf{b}_{LMN}^* \rangle = \langle \Delta(\mathbf{L}')_{IJK,LMN} \mathbf{b}_{IJK} \mathbf{b}_{LMN}^* \rangle = \Delta(\mathbf{L}')_{IJK,LMN} \mathbf{b}_{IJK} \mathbf{b}_{LMN}^* \quad (12)$$

Here,  $\Delta(\mathbf{L}')_{IJK,LMN}$  can be included in the orientational averaging since it is invariant under any rotation, and consequently, the averaging brackets may be removed as the value that is being averaged is a scalar. The hyperpolarizability tensor can be used in any coordinate frame (e.g. molecular frame bound to molecular symmetry elements).

Combining expressions (11) and (12), we get an expression for the rotation invariants in terms of Cartesian components of  $\mathbf{b}$ :

$$\mathbf{b}^2(\mathbf{L}) = \Delta(\mathbf{L})_{IJK,LMN} \mathbf{b}_{IJK} \mathbf{b}_{LMN}^*$$

The expressions for the invariants of a general (complex-valued) second harmonic hyperpolarizability tensor are given as follows:

$$\mathbf{b}_{1ss}^2 = \frac{1}{15\sqrt{3}} \left\{ 9 \sum_i |\mathbf{b}_{iii}|^2 + \sum_{i \neq j} \left[ 4 |\mathbf{b}_{ijj}|^2 + |\mathbf{b}_{jjj}|^2 + \text{Re}(6 \mathbf{b}_{iii} \mathbf{b}_{ijj}^* + 12 \mathbf{b}_{ijj} \mathbf{b}_{jjj}^* + 4 \mathbf{b}_{ijj} \mathbf{b}_{jii}^*) \right] + \sum_{i \neq j \neq k} \text{Re}(4 \mathbf{b}_{ijj} \mathbf{b}_{jkk}^* + \mathbf{b}_{ijj} \mathbf{b}_{ikk}^* + 4 \mathbf{b}_{ijj} \mathbf{b}_{kkj}^*) \right\}$$

$$\mathbf{b}_{1mm}^2 = \frac{1}{3\sqrt{3}} \left\{ \sum_{i \neq j} \left[ |\mathbf{b}_{ij}|^2 + |\mathbf{b}_{ji}|^2 - 2\text{Re}(\mathbf{b}_{ij} \mathbf{b}_{ji}^*) \right] + \sum_{i \neq j \neq k} \text{Re}(\mathbf{b}_{ij} \mathbf{b}_{kk}^* + \mathbf{b}_{ij} \mathbf{b}_{kk}^* - 2\mathbf{b}_{ij} \mathbf{b}_{jk}^*) \right\}$$

$$\mathbf{b}_{1sm+}^2 = -\frac{1}{3} \sqrt{\frac{2}{15}} \left\{ \sum_{i \neq j} \left[ 2|\mathbf{b}_{ij}|^2 - |\mathbf{b}_{ji}|^2 + \text{Re}(3\mathbf{b}_{ij} \mathbf{b}_{jj}^* - 3\mathbf{b}_{ii} \mathbf{b}_{ij}^* - \mathbf{b}_{ij} \mathbf{b}_{ji}^*) \right] + \sum_{i \neq j \neq k} \text{Re}(2\mathbf{b}_{ij} \mathbf{b}_{kk}^* - \mathbf{b}_{ij} \mathbf{b}_{kk}^* - \mathbf{b}_{ij} \mathbf{b}_{jk}^*) \right\}$$

$$\mathbf{b}_{1sm-}^2 = -i \sqrt{\frac{2}{15}} \left\{ \sum_{i \neq j} \text{Im}(\mathbf{b}_{ii} \mathbf{b}_{ij}^* + \mathbf{b}_{ij} \mathbf{b}_{jj}^* + \mathbf{b}_{ij} \mathbf{b}_{ji}^*) + \sum_{i \neq j \neq k} \text{Im}(\mathbf{b}_{ij} \mathbf{b}_{kk}^*) \right\}$$

$$\mathbf{b}_{2mm}^2 = \frac{1}{3\sqrt{5}} \left\{ \sum_{i \neq j} \left[ |\mathbf{b}_{ij}|^2 + |\mathbf{b}_{ji}|^2 + 2\text{Re}(\mathbf{b}_{ij} \mathbf{b}_{ji}^*) \right] + \sum_{i \neq j \neq k} \left[ 2|\mathbf{b}_{ijk}|^2 + \text{Re}(2\mathbf{b}_{ij} \mathbf{b}_{kk}^* - \mathbf{b}_{ij} \mathbf{b}_{kk}^* - \mathbf{b}_{ij} \mathbf{b}_{kj}^* - 2\mathbf{b}_{ijk} \mathbf{b}_{jki}^*) \right] \right\}$$

$$\mathbf{b}_{3ss}^2 = \frac{1}{15\sqrt{7}} \left\{ 6 \sum_i |\mathbf{b}_{iii}|^2 + \sum_{i \neq j} \left[ 16|\mathbf{b}_{ij}|^2 + 4|\mathbf{b}_{ji}|^2 + \text{Re}(16\mathbf{b}_{ij} \mathbf{b}_{ji}^* - 6\mathbf{b}_{ii} \mathbf{b}_{ij}^* - 12\mathbf{b}_{ij} \mathbf{b}_{jj}^*) \right] + \sum_{i \neq j \neq k} \left[ 5|\mathbf{b}_{ij}|^2 + \text{Re}(10\mathbf{b}_{ijk} \mathbf{b}_{jki}^* - 4\mathbf{b}_{ij} \mathbf{b}_{kk}^* - \mathbf{b}_{ij} \mathbf{b}_{kk}^* - 4\mathbf{b}_{ij} \mathbf{b}_{kk}^*) \right] \right\}$$

The summation should be done over  $x$ ,  $y$ , and  $z$  for all indices  $i, j, k$ .

We now consider a few important special cases. For systems with  $C_{2v}$  symmetry, such as pNA and  $\Lambda$ -shaped molecules, the main invariants will take the form

$$\mathbf{b}_{1ss}^2(C_{2v}) = \frac{1}{15\sqrt{3}} \left| 3\mathbf{b}_{zzz} + 2(\mathbf{b}_{xxz} + \mathbf{b}_{yyz}) + \mathbf{b}_{zxx} + \mathbf{b}_{zyy} \right|^2$$

$$\mathbf{b}_{1mm}^2(C_{2v}) = \frac{1}{3\sqrt{3}} \left| \mathbf{b}_{xxz} + \mathbf{b}_{yyz} - \mathbf{b}_{zxx} - \mathbf{b}_{zyy} \right|^2$$

$$\mathbf{b}_{2mm}^2(C_{2v}) = \frac{1}{3\sqrt{5}} \left| \mathbf{b}_{xxz} - \mathbf{b}_{yyz} - \mathbf{b}_{zxx} + \mathbf{b}_{zyy} \right|^2$$

$$\mathbf{b}_{3ss}^2(C_{2v}) = \frac{2}{15\sqrt{7}} \left\{ 3|\mathbf{b}_{zzz}|^2 + 8(|\mathbf{b}_{xxz}|^2 + |\mathbf{b}_{yyz}|^2) + 2(|\mathbf{b}_{zxx}|^2 + |\mathbf{b}_{zyy}|^2) + \text{Re} \left[ 8(\mathbf{b}_{xxz} \mathbf{b}_{zxx}^* + \mathbf{b}_{yyz} \mathbf{b}_{zyy}^*) - 6(\mathbf{b}_{xxz} \mathbf{b}_{zzz}^* + \mathbf{b}_{yyz} \mathbf{b}_{zzz}^*) - 3(\mathbf{b}_{zzz} \mathbf{b}_{zxx}^* + \mathbf{b}_{zzz} \mathbf{b}_{zyy}^*) - 2(\mathbf{b}_{xxz} \mathbf{b}_{zyy}^* + \mathbf{b}_{yyz} \mathbf{b}_{zxx}^*) - 4\mathbf{b}_{xxz} \mathbf{b}_{yyz}^* - \mathbf{b}_{zxx} \mathbf{b}_{zyy}^* \right] \right\}$$

The other symmetries that may be important in relation to measurements for crystal violet are  $C_3$ ,  $D_3$  and  $D_{3h}$ . The figures of merit for a system with  $C_3$  symmetry are given by

$$\begin{aligned} \mathbf{b}_{1ss}^2(C_3) &= \frac{1}{15\sqrt{3}} |3\mathbf{b}_{zzz} + 2\mathbf{b}_{xxz} + 2\mathbf{b}_{zxx}|^2 \\ \mathbf{b}_{1mm}^2(C_3) &= \frac{4}{3\sqrt{3}} |\mathbf{b}_{xxz} - \mathbf{b}_{zxx}|^2 \\ \mathbf{b}_{2mm}^2(C_3) &= \frac{4}{\sqrt{5}} |\mathbf{b}_{xyz}|^2 \\ \mathbf{b}_{1ss}^2(C_3) &= \frac{2}{15\sqrt{7}} \left[ 30(|\mathbf{b}_{xxx}|^2 + |\mathbf{b}_{yyy}|^2) + 3|\mathbf{b}_{zzz}|^2 + 12|\mathbf{b}_{xxz}|^2 + \right. \\ &\quad \left. + \text{Re}(12\mathbf{b}_{xxz}\mathbf{b}_{zxx}^* - 12\mathbf{b}_{xxz}\mathbf{b}_{zzz}^* - 6\mathbf{b}_{zzz}\mathbf{b}_{zxx}^*) \right] \end{aligned}$$

$D_3$  systems have only two distinguishable components in both Cartesian and irreducible representations:

$$\mathbf{b}_{1ss}^2(D_3) = \mathbf{b}_{1mm}^2(D_3) = 0; \quad \mathbf{b}_{2mm}^2(D_3) = \frac{4}{\sqrt{5}} |\mathbf{b}_{xyz}|^2; \quad \mathbf{b}_{3ss}^2(D_3) = \frac{4}{\sqrt{7}} |\mathbf{b}_{xxx}|^2$$

while a higher  $D_{3h}$  symmetry eliminates Kleinman disallowed component leaving only octupolar part non-vanishing. The results of our measurements for crystal violet argue against the  $D_3$  or  $D_{3h}$  configurations, as there is a significant contribution from two vector parts that must not appear in systems with these symmetries.

## Appendix B

It has been discussed above that any  $90^\circ$  measurement is not sufficient for measuring the entire set of rotation invariants of hyperpolarizability tensor. However, many sources quote the depolarization ratio as a standard value experimentally determined via  $90^\circ$  HRS experiments. Consequently, it may be useful to express the depolarization ratio in terms of the rotational invariants determined from a  $45^\circ$  experiment. The general formalism presented in the theoretical part of this paper can be used to determine the scattering intensity for any geometry of the experiment. Defining the input and output polarization vectors for a  $90^\circ$  experiment (linearly polarized) as

$$\hat{e}_i = \hat{e}_i^* = \hat{y}; \quad \hat{e}_o = \hat{e}_o^* = \begin{cases} \hat{y}, & \mathbf{P} \\ \hat{z}, & \perp \end{cases}$$

and substituting it into equations (6), one gets rather simple expressions for the scattered intensities in the cases of parallel and perpendicular configurations:

$$\begin{aligned}
 I_{\perp} &= \frac{1}{9}c_{1ss} \mathbf{b}_{1ss}^2 + \frac{4}{9}c_{1mm} \mathbf{b}_{1mm}^2 + \frac{4}{9}c_{1sm+} \mathbf{b}_{1sm+}^2 + \left(\frac{4}{9}c_{2mm} + \frac{2}{3}c'_{2mm}\right) \mathbf{b}_{2mm}^2 + \left(\frac{1}{3}c_{3ss} + \frac{1}{9}c'_{3ss}\right) \mathbf{b}_{3ss}^2 \\
 &= \frac{1}{15\sqrt{3}} \mathbf{b}_{1ss}^2 + \frac{1}{3\sqrt{3}} \mathbf{b}_{1mm}^2 + \frac{1}{3}\sqrt{\frac{2}{15}} \mathbf{b}_{1sm+}^2 + \frac{1}{3\sqrt{5}} \mathbf{b}_{2mm}^2 + \frac{4}{15\sqrt{7}} \mathbf{b}_{3ss}^2 \\
 I_{\mathbf{P}} &= c_{1ss} \mathbf{b}_{1ss}^2 + (c_{3ss} + c'_{3ss}) \mathbf{b}_{3ss}^2 = \frac{\sqrt{3}}{5} \mathbf{b}_{1ss}^2 + \frac{2}{5\sqrt{7}} \mathbf{b}_{3ss}^2
 \end{aligned}$$

Now, one can calculate the value of the depolarization ratio that should be expected for a material with a given set of invariants  $\mathbf{b}_{\mathbf{L}}^2$ .

## References

- [1] *Molecular Nonlinear Optics*, J. Zyss, ed. (Academic Press, 1994).
- [2] *Polymers for Second-Order Nonlinear Optics*, G. Lindsay and K. Singer, eds. (ACS Symp. Ser. 601, 1995).
- [3] D.A. Kleinman, "Nonlinear Dielectric Polarization in Optical Media", *Phys. Rev.* **126**, 1977-1979 (1962).
- [4] K.D. Singer, S.F. Hubbard, A. Schober, L. M. Hayden, and K. Johnson, "Second Harmonic Generation" in *Characterization Techniques and Tabulations for Organic Nonlinear Optical Materials*, M.G. Kuzyk and C.W. Dirk, eds., 311-513 (Marcel Dekker, 1998).
- [5] J. Zyss and I. Ledoux, "Nonlinear Optics in Multipolar Media: Theory and Experiment", *Chem. Rev.* **94**, 77-105 (1994).
- [6] S. Brasselet and J. Zyss, "Multipolar Molecules and Multipolar Fields: Probing and Controlling the Tensorial Nature of Nonlinear Molecular Media", *J. Opt. Soc. Am. B.* **15**, 257-288 (1998).
- [7] M. Joffre, D. Yaron, R. Silbey, and J. Zyss, "Second-Order Optical Nonlinearity in Octopolar Aromatic Systems", *J. Chem. Phys.* **97**, 5607-5615 (1992).
- [8] T. Verbiest, K. Clays, C. Samyn, J. Wolff, D. Reinhoudt, and A. Persoons, "Investigations of the Hyperpolarizability in Organic Molecules from Dipolar to Octopolar Systems", *J. Am. Chem. Soc.* **116**, 9320-9323 (1994).
- [9] S. F. Hubbard, R.G. Petschek, K.D. Singer, N. D'Sidocky, C. Hudson, L.C. Chien, C.C. Henderson, and P.A. Cahill, "Measurements of Kleinman-disallowed

- Hyperpolarizability in Conjugated Chiral Molecules”, *J. Opt. Soc. Am. B* **15**, 289-301 (1998).
- [10] M. Kozirowski, “Electric-Dipole Differential Hyper-Rayleigh and Hyper-Raman Scattering of Elliptically Polarized Light”, *Phys. Rev. A* **31**, 509-510 (1985); G. Wagniere, “Theoretical Investigation of Kleinman Symmetry in Molecules”, *Appl. Phys. B* **41**, 169-172 (1986).
- [11] R. Wortmann, P. Krämer, C. Glania, S. Lebus, and N. Detzer, “Deviations from Kleinman Symmetry of the Second-Order Polarizability Tensor in Molecules with Low-Lying Perpendicular Electronic Bands”, *Chem. Phys.* **173**, 99-108 (1992).
- [12] V. Ostroverkhov, O. Ostroverkhova, R.G. Petschek, and K.D. Singer, L. Sukhomlinova, R.J. Twieg S.-X. Wang and L.C. Chien, “Optimization of the Molecular Hyperpolarizability for Second Harmonic Generation in Chiral Media”, submitted.
- [13] I. D. Morrison, R. G. Denning, W. M. Laidlaw and M. A. Stammers, “Measurement of First Hyperpolarizabilities by Hyper-Rayleigh Scattering”, *Rev. Sci. Instrum.* **67**, 1445-1453 (1996).
- [14] P. Kaatz and D. P. Shelton, “Polarized Hyper-Rayleigh Light Scattering Measurements of Nonlinear Optical Chromophores”, *J. Chem. Phys.* **105**, 3918-3929 (1996).
- [15] T. W. Chui and K. Y. Wong, “Study of Hyper-Rayleigh Scattering and Two-Photon Absorption Induced Fluorescence from Crystal Violet”, *J. Chem. Phys.* **109**, 1391-1396 (1998).
- [16] S.J. Lalama and A.F. Garito, “Origin of the Nonlinear Second-Order Optical Susceptibilities of Organic Systems,” *Phys. Rev. A* **20**, 1179-1194 (1979).
- [17] G.J.T. Heesink, A.G.T. Ruiter, N.F. van Hulst, and B. Bölger, “Determination of Hyperpolarizability Tensor Components by Hyper-Rayleigh Scattering”, *Phys. Rev. Lett.* **71**, 999-1002 (1993).
- [18] X-ray crystal structures were determined by Dr. C. Barnes at University of Missouri-Columbia.

- [19] J. Zyss, T. C. Van, C. Dhenaut and I. Ledoux, "Harmonic Rayleigh Scattering from Nonlinear Octupolar Molecular Media: the Case of Crystal Violet", *J. Chem. Phys.* **177**, 281-296 (1993).
- [20] S. Stadler, R. Dietrich, G. Bourhill, and Ch. Bräuchle, "Long-Wavelength First Hyperpolarizability Measurements by Hyper-Rayleigh Scattering", *Opt. Lett.* **21**, 251-253 (1996).
- [21] H. B. Lueck, J. L. McHale and W. D. Edwards, "Symmetry-Breaking Solvent Effects on the Electronic Structure and Spectra of a Series of Triphenylmethane Dyes", *J. Am. Chem. Soc.*, **114**, 2342-2348 (1992).
- [22] Y. Maruyama, M. Ishikawa, and H. Satozono, "Femtosecond Isomerization of Crystal Violet in Alcohols", *J. Am. Chem. Soc.* **118**, 6257-6263 (1996).

**Table 1.** Irreducible tensors used in the decomposition (with normalization coefficients)<sup>#</sup>.

$\Delta(\mathbf{L})$	Explicit form	$c$	$c'$
$\Delta(0aa)$	$c\mathbf{e}_{ijk}\mathbf{e}_{lmn}$	1/6	-
$\Delta(1ss)$	$c\mathbf{P}_s\bar{  }\mathbf{P}_s$	$\sqrt{3}/5$	-
$\Delta(1mm)$	$c\mathbf{P}_m\bar{  }\mathbf{P}_m$	$\sqrt{3}/4$	-
$\Delta(1m'm')$	$c\mathbf{P}_{m'}\underline{  }\mathbf{P}_{m'}$	$1/\sqrt{3}$	-
$\Delta(1sm+)$	$c(\mathbf{P}_m\bar{  }\mathbf{P}_s + \mathbf{P}_s\bar{  }\mathbf{P}_m)$	$\sqrt{3/40}$	-
$\Delta(1sm-)$	$c(\mathbf{P}_m\bar{  }\mathbf{P}_s - \mathbf{P}_s\bar{  }\mathbf{P}_m)$	$\sqrt{3/40}$	-
$\Delta(1sm'+)$	$c(\mathbf{P}_s\underline{  }\mathbf{P}_{m'} + \mathbf{P}_{m'}\underline{  }\mathbf{P}_s)$	$1/\sqrt{10}$	-
$\Delta(1sm'-)$	$c(\mathbf{P}_s\underline{  }\mathbf{P}_{m'} - \mathbf{P}_{m'}\underline{  }\mathbf{P}_s)$	$1/\sqrt{10}$	-
$\Delta(1mm'+)$	$c(\mathbf{P}_{m'}\underline{  }\mathbf{P}_m + \mathbf{P}_m\underline{  }\mathbf{P}_{m'})$	$1/\sqrt{2}$	-
$\Delta(1mm'-)$	$c(\mathbf{P}_{m'}\underline{  }\mathbf{P}_m - \mathbf{P}_m\underline{  }\mathbf{P}_{m'})$	$1/\sqrt{2}$	-
$\Delta(2mm)$	$c(\mathbf{P}_m\bar{  }\mathbf{P}_m) + c'(\mathbf{P}_m\bar{\times}\mathbf{P}_m)$	$-3/(4\sqrt{5})$	$1/\sqrt{5}$
$\Delta(2m'm')$	$c(\mathbf{P}_{m'}\underline{  }\mathbf{P}_{m'}) + c'(\mathbf{P}_{m'}\underline{\times}\mathbf{P}_{m'})$	$-1/\sqrt{5}$	$2/\sqrt{5}$
$\Delta(2mm'+)$	$c(\mathbf{P}_m\underline{  }\mathbf{P}_{m'} + \mathbf{P}_{m'}\underline{  }\mathbf{P}_m) + c'(\mathbf{P}_m\underline{\times}\mathbf{P}_{m'} + \mathbf{P}_{m'}\underline{\times}\mathbf{P}_m)$	$\sqrt{3/10}$	$-\sqrt{2/15}$
$\Delta(2mm'-)$	$c(\mathbf{P}_m\underline{  }\mathbf{P}_{m'} - \mathbf{P}_{m'}\underline{  }\mathbf{P}_m) + c'(\mathbf{P}_m\underline{\times}\mathbf{P}_{m'} - \mathbf{P}_{m'}\underline{\times}\mathbf{P}_m)$	$\sqrt{3/10}$	$-\sqrt{2/15}$
$\Delta(3ss)$	$c(\mathbf{P}_s\equiv) + c'\mathbf{P}_s\bar{  }\mathbf{P}_s$	$1/\sqrt{7}$	$-3/(5\sqrt{7})$

<sup>#</sup> The graphs represent various combinations of Kronecker  $\delta$ s as  $\bar{||} = \begin{smallmatrix} i & - & l \\ j & | & m \\ k & | & n \end{smallmatrix} \equiv d_{ij}d_{jk}d_{ln}$ .

**Table 2.** Rotation invariants with respect to Kleinman allowed vector part.

Material (wavelength)	$\beta^2_{1mm}/\beta^2_{1ss}$	$\beta^2_{1sm+}/\beta^2_{1ss}$	$\beta^2_{1sm-}/\beta^2_{1ss}$	$\beta^2_{2mm}/\beta^2_{1ss}$	$\beta^2_{3ss}/\beta^2_{1ss}$	$\beta^2_{1ss}/(\beta^2_{1ss})_{pNA}$
1064 nm						
1 – pNA	0.16±0.08	-0.02±0.03	0.17±0.02	0.04±0.04	0.54±0.04	1
2	0.22±0.04	0.11±0.02	-0.05±0.01	0.11±0.05	0.52±0.03	~8.5
5	0.6±0.2	0.05±0.01	0.25±0.01	0.02±0.02	0.41±0.02	~82
6 - Q-BNH	0.15±0.10	-0.06±0.07	0.13±0.03	0.19±0.05	0.47±0.04	~11.5
7	0.13±0.03	0.10±0.02	0.15±0.02	0.08±0.02	0.51±0.02	~8.7
8 – CV	1.2±0.2	-1.3±0.1	0.08±0.03	0.8±0.2	1.7±0.2	~712
1340 nm						
1 – pNA	0.18±0.05	-0.03±0.02	0.057±0.002	0.00±0.05	0.53±0.02	1
3	0.05±0.01	0.04±0.01	0.04±0.01	0.11±0.06	0.47±0.01	~31.4
4	0.11±0.02	0.13±0.01	0.01±0.01	0.00±0.01	0.40±0.01	~93.6

**Table 3.** Figures of merit of the four irreducible components of  $\beta$  tensor (esu).

Material (Wavelength)	$\ \beta_{1ss}\ $ , $\times 10^{-30}$ esu	$\ \beta_{1mm}\ $ , $\times 10^{-30}$ esu	$\ \beta_{2mm}\ $ , $\times 10^{-30}$ esu	$\ \beta_{3ss}\ $ , $\times 10^{-30}$ esu
1064nm				
1 - pNA	11.2 $\pm$ 1.6	4.6 $\pm$ 1.2	2.1 $\pm$ 2.6	8.2 $\pm$ 1.2
2	33.2 $\pm$ 4.8	15.5 $\pm$ 2.6	10.8 $\pm$ 2.9	23.9 $\pm$ 3.5
5	110 $\pm$ 16	26.8 $\pm$ 6.0	15.7 $\pm$ 7.6	70 $\pm$ 10
6 - Q-BNH	38.3 $\pm$ 5.9	14.7 $\pm$ 5.7	16.9 $\pm$ 3.3	26.3 $\pm$ 4.3
7	33.6 $\pm$ 4.7	12.1 $\pm$ 2.2	9.6 $\pm$ 1.6	23.9 $\pm$ 3.4
8 - CV	305 $\pm$ 58	341 $\pm$ 72	276 $\pm$ 52	398 $\pm$ 81
1340nm				
pNA	8.1 $\pm$ 1.5	3.4 $\pm$ 0.8	0.0 $\pm$ 1.9	5.9 $\pm$ 1.1
3	44.9 $\pm$ 7.7	10.2 $\pm$ 1.9	14.7 $\pm$ 4.8	30.9 $\pm$ 5.3
4	78 $\pm$ 13	25.7 $\pm$ 4.7	0.0 $\pm$ 1.0	49.1 $\pm$ 8.4

**Table 4.** Rotational invariants of CV in different solvents.

Material	$\beta^2_{1mm}/\beta^2_{1ss}$	$\beta^2_{1sm+}/\beta^2_{1ss}$	$\beta^2_{1sm-}/\beta^2_{1ss}$	$\beta^2_{2mm}/\beta^2_{1ss}$	$\beta^2_{3ss}/\beta^2_{1ss}$
CV/acetone	1.2±0.2	-1.3±0.1	0.08±0.03	0.8±0.2	1.7±0.2
CV/methanol	0.5±0.2	-0.9±0.1	-0.22±0.04	1.1±0.1	1.3±0.2
CV/dioxane	0.9±0.2	-0.8±0.2	0.29±0.02	0.90±0.03	1.9±0.3

**Figure 1.** HRS experiment with arbitrary ellipticity of incoming and outgoing polarizations.

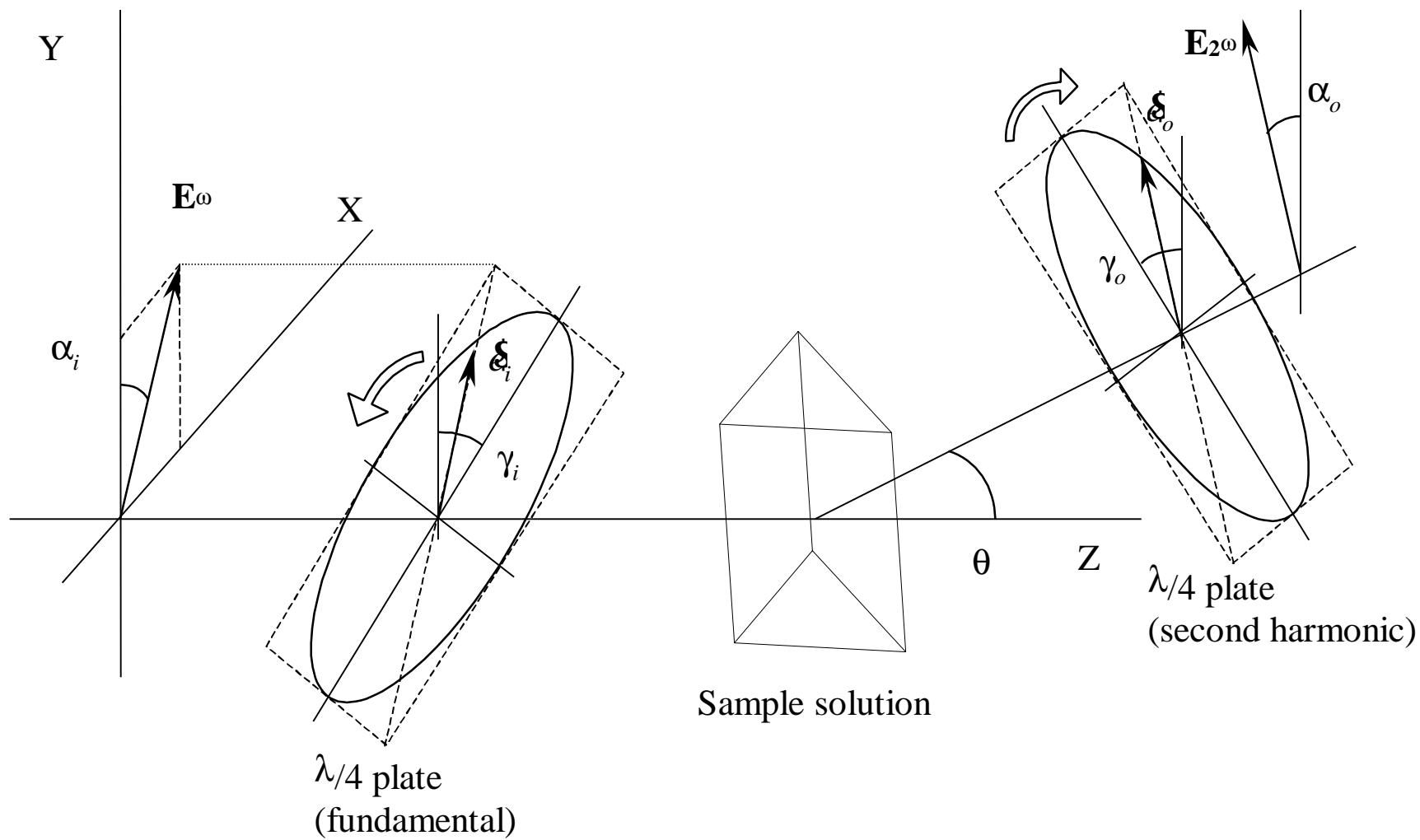
**Figure 2.** Experimental setup for 45° hyper-Rayleigh scattering experiment.

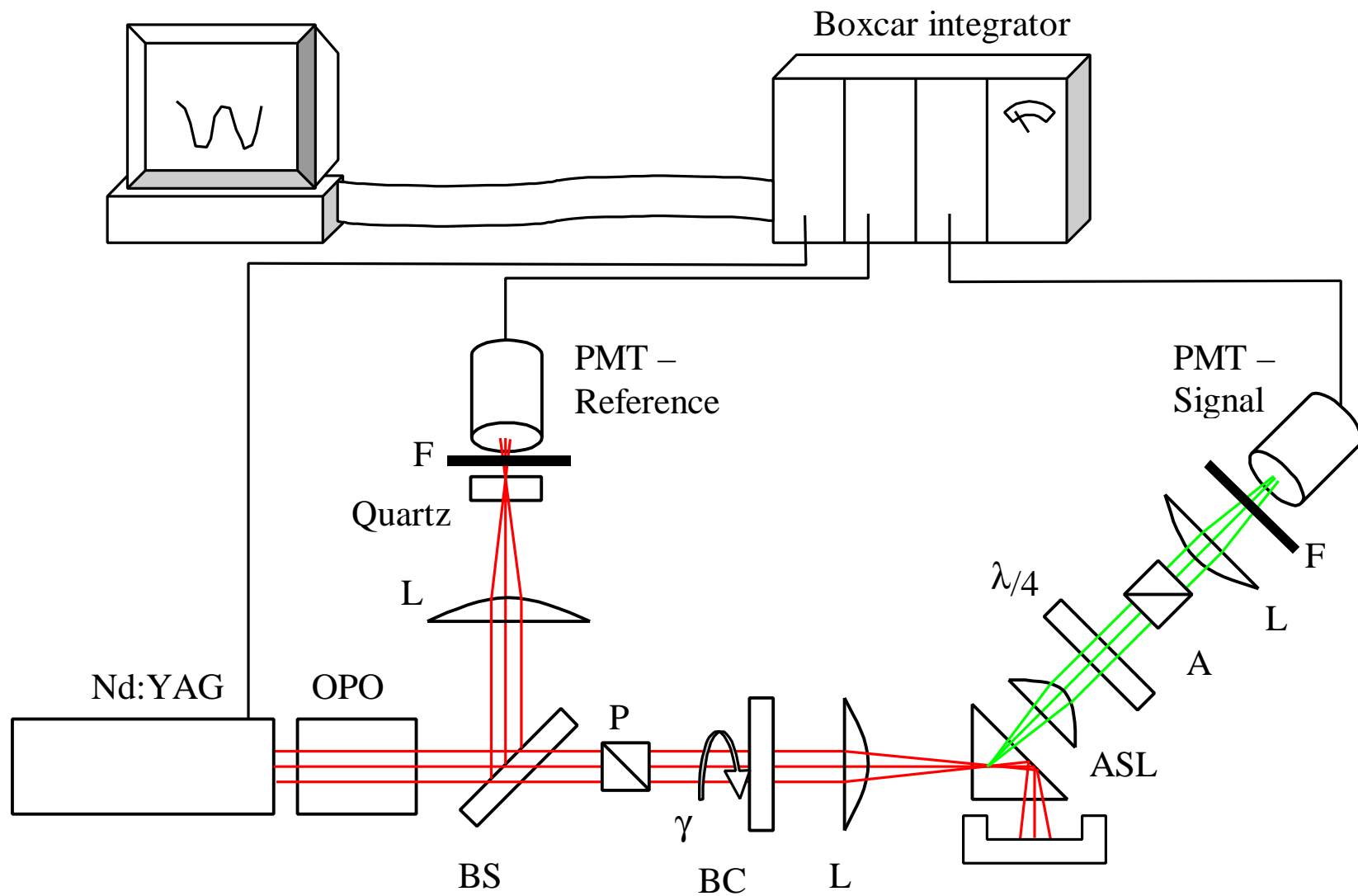
P – input polarizer, BS – beamsplitter, L – lenses, BC – Berek compensator, ASL – aspherical lens,  $\lambda/4$  – quarter-wave plate, A – output polarizer, PMT – photomultiplier tubes, F – filters.

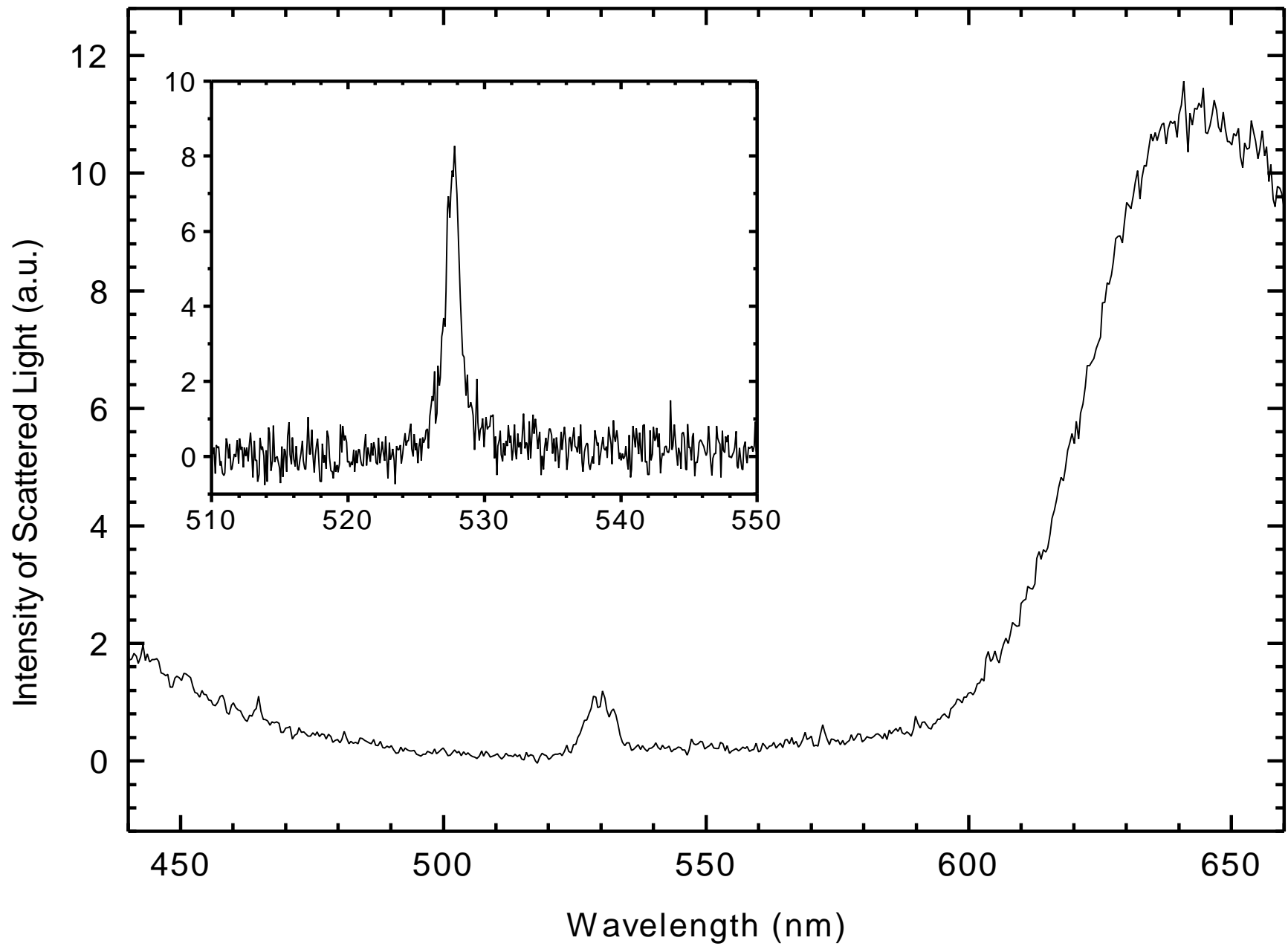
**Figure 3.** Spectral content of the light scattered from solution of crystal violet in acetone (main graph – 300 grooves/mm; inset – 1200 grooves/mm grating)

**Figure 4.** Molecular structures of the studied molecules (with first excited state absorption maximum wavelengths)

**Figure 5.** Polar plots of typical data points with fitted curve for (a) pNA, (b) Q-BNH, and (c) crystal violet.

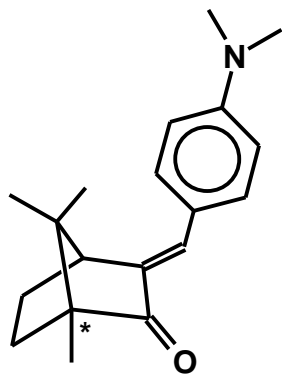




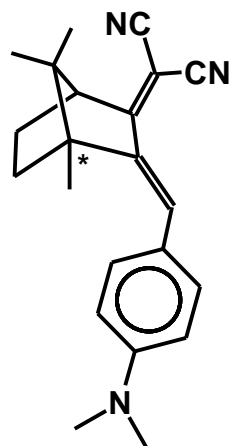




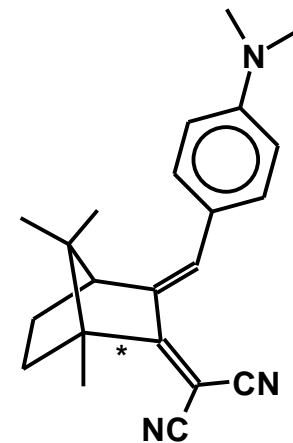
1-pNA (366nm)



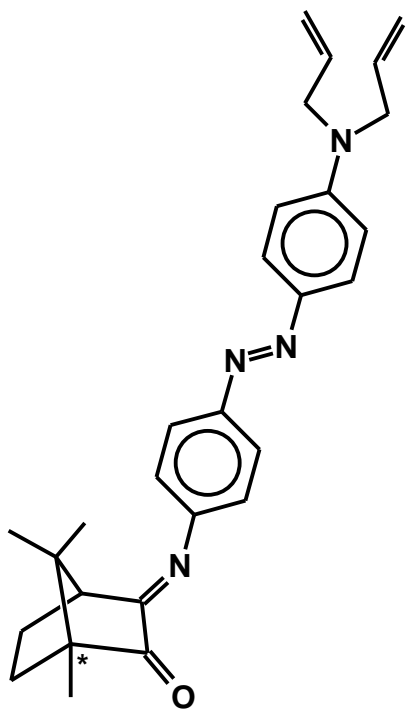
2-(367nm)



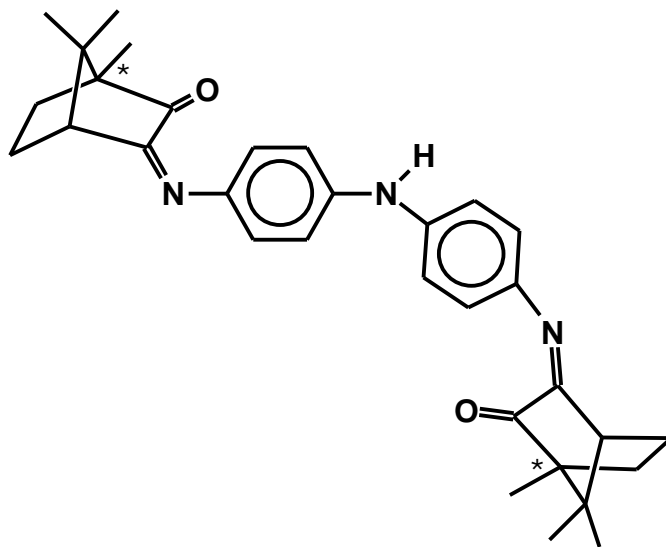
3-(467nm)



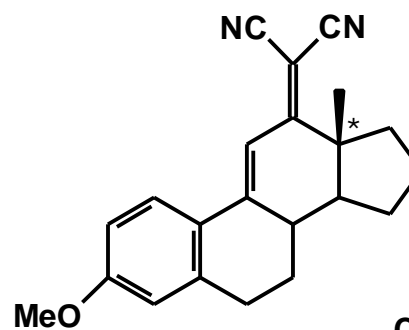
4-(473nm)



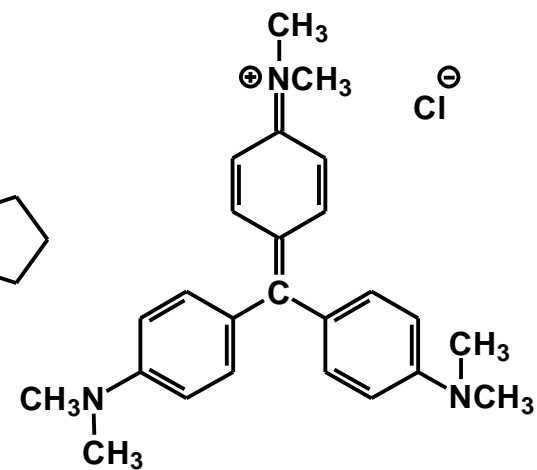
5-(427nm)



6-Q-BNH (425nm)



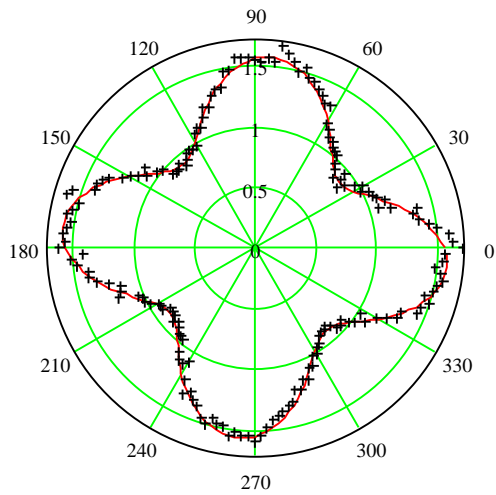
7-(397nm)



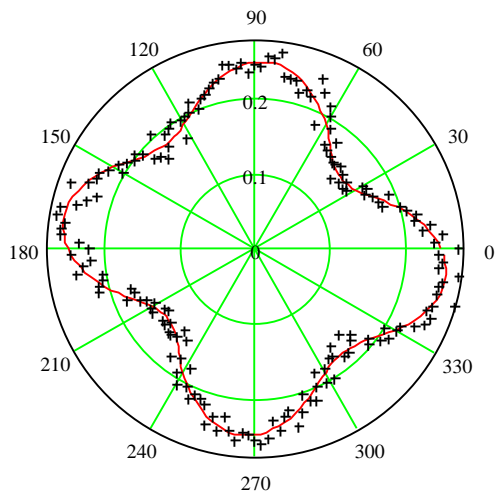
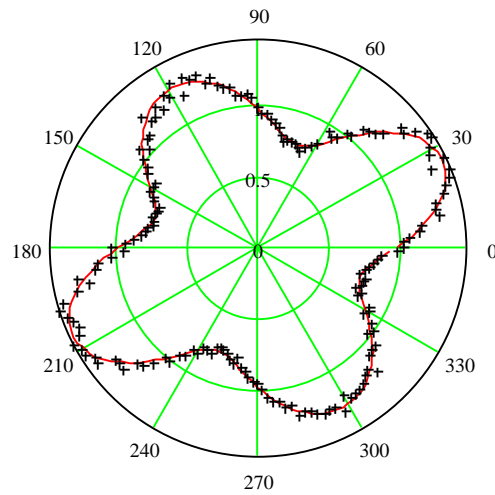
8-CV (588nm)

$$a_o = 57.8^\circ; \epsilon_o = 75.3^\circ$$

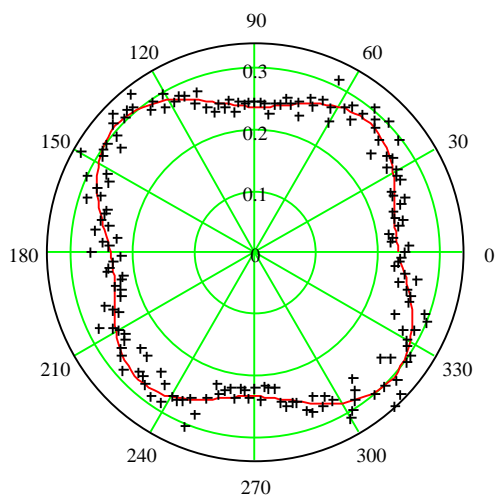
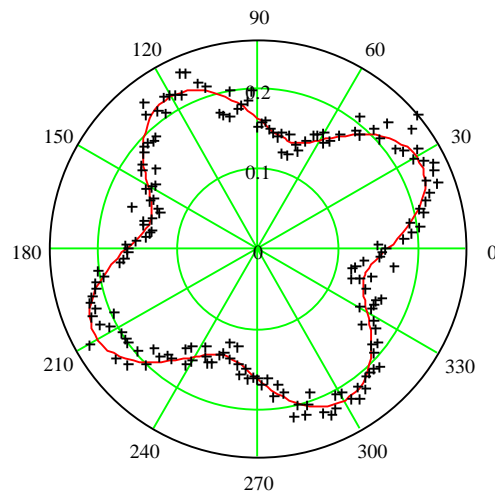
$$a_o = \epsilon_o = -30.4^\circ$$



(a)



(b)



(c)

